Resource-Competing Oscillator Network as a Model of Amoeba-Based Neurocomputer

Masashi Aono[1], Yoshito Hirata[2], Masahiko Hara[1], and Kazuyuki Aihara[2,3]

[1] Flucto-Order Functions Asian Collaboration Team, Advanced Science Institute, RIKEN, Wako, Saitama 351-0198, Japan
[2] Institute of Industrial Science, The University of Tokyo, Meguro-ku, Tokyo 153-8505, Japan
[3] ERATO Aihara Complexity Modelling Project, JST, Shibuya-ku, Tokyo 151-0064, Japan
masashi.aono@riken.jp

Abstract. An amoeboid organism, *Physarum*, exhibits rich spatiotemporal oscillatory behavior and various computational capabilities. Previously, the authors created a recurrent neurocomputer incorporating the amoeba as a computing substrate to solve optimization problems. In this paper, considering the amoeba to be a network of oscillators coupled such that they compete for constant amounts of resources, we present a model of the amoeba-based neurocomputer. The model generates a number of oscillation modes and produces not only simple behavior to stabilize a single mode but also complex behavior to spontaneously switch among different modes, which reproduces well the experimentally observed behavior of the amoeba. To explore the significance of the complex behavior, we set a test problem used to compare computational performances of the oscillation modes. The problem is a kind of optimization problem of how to allocate a limited amount of resource to oscillators such that conflicts among them can be minimized. We show that the complex behavior enables to attain a wider variety of solutions to the problem and produces better performances compared with the simple behavior.

Keywords: Physarum, Amoeba-based Computing, Resource Allocation.

1 Introduction

A single-celled amoeboid organism, the true slime mold *Physarum polycephalum* (Fig. 1A), has been studied actively in recent years to explore and exploit its notable computational capabilities. Nakagaki and co-workers showed that the amoeba is capable of searching for optimal paths between foods [1,2,3] and anticipating periodic events [4].

In the amoeba's body, a constant amount of intracellular protoplasmic sol flows through tubular channels in a shuttle-wise manner, as its extracellular gel layer like a sponge (ectoplasm) oscillates the contraction tension rhythmically to squeeze and absorb the sol (Fig. 1B). To observe the dependences of the amoeba's spatiotemporal oscillation modes on geometric constraints, Takamatsu

C.S. Calude et al. (Eds.): UC 2009, LNCS 5715, pp. 56–69, 2009.

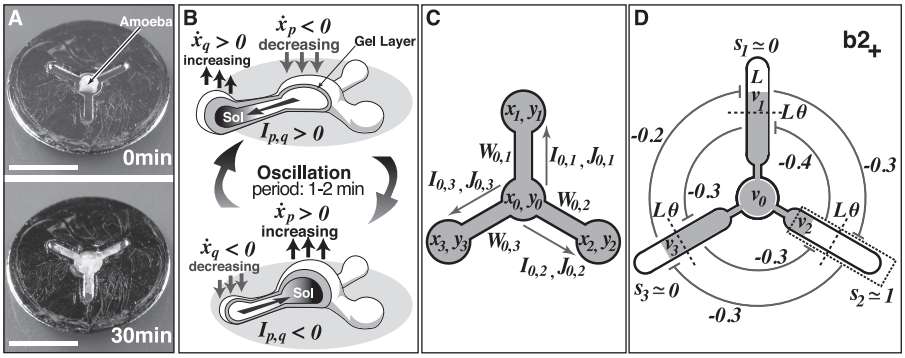

Fig. 1. (A) An individual *Physarum* amoeba in an Au-coated plastic chamber on an agar plate (scale bar = 7 mm). The amoeba acts only inside the chamber due to its aversion to Au. In the absence of light stimulation, the spherically shaped amoeba (top) flattened to elongate its three branches (bottom) by keeping its total volume almost constant. (B) The amoeba's body architecture. (C) Schematic diagram of the model in which the volumes of the amoeba's branches (nodes) are stationary. (D) Schematic diagram of the model that takes into account the growth/degeneration of the branches. Due to inhibitory feedback, branch 2 is stressed by light $s_2 \simeq 1$ (dotted rectangle) as branches 1 and 3 grow beyond the critical level $L\theta$ (broken lines).

and co-workers placed the amoeba in a chamber patterned as a ring network with several nodes [5,6]. The amoeba's body part in each node is regarded as an oscillator because its vertical thickness oscillates. In a two-oscillator chamber, the amoeba showed antiphase synchronization. Circularly coupled three oscillators exhibited rotation modes, partial in-phase and partial antiphase synchronization modes. Interestingly, after maintaining each of these modes for several periods, the amoeba spontaneously switched among different modes even though no external perturbation was applied [7].

The amoeba shows a photoavoidance response to degenerate its branches when illuminated by light. Introducing optical feedback applied according to a recurrent neural network model, Aono and co-workers created a neurocomputer employing the amoeba as a solution searcher of optimization problems [8,9,10,11]. In previous works [12,13], the amoeba's branches were induced to grow or degenerate in a network-patterned chamber in search of an optimal solution to the Traveling Salesman Problem (TSP). It was shown that the system was capable of reaching the optimal solution of the four-city TSP with a high probability.

In the solution-searching processes, the amoeba showed various oscillation modes and *spontaneous switching* among them. Depending on the oscillation modes, the performances in finding the solution seemed to vary. This dependence, however, could not be verified experimentally because it is hard to control the amoeba's oscillation mode. Thus, we create a model that produces different oscillation modes by changing parameters. Setting a problem derived from TSP, we explore the relationships between the oscillation modes and performances.

2 Models

2.1 Resource-Competing Oscillator Network

We model the amoeba as a network of oscillators coupled such that the sums of their variables are kept constant while resources are exchanged competitively. Consider a graph $G(Q, E)$ with a set of nodes Q and a set of edges E, where Q contains M nodes. Let $v_q(t) \in \mathbb{R}$ and $x_q(t) \in \mathbb{R}$ be a *volume* of node q and its *rate of change*, respectively. That is,

$$\dot{v_q} = x_q. \tag{1}$$

We define the dynamics of x_q in accordance with Kirchhoff's current law. Namely, the increment of x_q is supplied as the sum of resources flown from its coupled nodes:

$$\dot{x_q} = \sum_{p \in P_q} I_{p,q}, \tag{2}$$

where $I_{p,q}$ is a *current of resource* flowing from node p to q, and P_q is a set of all nodes connected to node q. Owing to the symmetry in currents $I_{p,q} = -I_{q,p}$, the sum of all increments for x vanishes: $\sum_{q \in Q} \dot{x_q} = \sum_{(p,q) \in E} I_{p,q} + I_{q,p} = 0$. This property keeps $\sum_{q \in Q} x_q$ constant. Thus, if we set the initial states $x_q(0)$ such that $\sum_{q \in Q} x_q(0) = 0$, the sum of the volumes $\sum_{q \in Q} v_q$ is conserved. This corresponds to a condition that a constant amount of protoplasmic sol flowing inside the amoeba is shared by a number of branches.

Each node q has its own *intranode dynamics* defined as the following two-variable oscillator to generate a regular rotation on a x-y plane $\mathbb{R} \times \mathbb{R}$:

$$\dot{x_q^*} = f(r_q\ x_q - y_q - x_q(x_q^2 + y_q^2)), \tag{3}$$

$$\dot{y_q^*} = f(x_q + r_q\ y_q - y_q(x_q^2 + y_q^2)), \tag{4}$$

where f adjusts a *frequency*, and r_q sets an *amplitude* (*radius*) to be $\sqrt{r_q}$. This oscillator produces stable limit-cycle and was taken from a standard form of super-critical Hopf bifurcation [14]. The variables x and y might be considered as representing the concentrations of *activator* and *inhibitor* in a reduced model of the amoeba's intracellular biochemical oscillation, respectively. However, this oscillator would be insufficient to give a physiologically valid model. We chose the oscillator just because it simply produces a pure rotation that allows us to concentrate on complex behavior generated by coupling the simple dynamics.

To determine currents $I_{p,q}$ in Eq. (2), each node q requires that the *actual volume change* $\dot{x_q}$ becomes closer to the *expected demand* $\dot{x_q^*}$ of the *intranode dynamics* Eq. (3). Additionally, currents $I_{p,q}$ are required to flow from smaller-incremented to larger-incremented nodes to represent the competitive *internode relationships* in the amoeba (Fig. 1B). That is, the protoplasmic sol flows from a contracting (squeezing) site to a relaxing (absorbing) site of the sponge-like gel layer so that the pressure difference between the two sites is widened further. To

balance these *intranode* and *internode* requirements, currents $I_{p,q}$ are determined to minimize the following object function H_I:

$$H_I = \lambda \sum_{q\in Q} \Big(\dot{x^*_q} - \sum_{p\in P_q} I_{p,q}\Big)^2 + (1-\lambda) \sum_{(p,q)\in E} \big(W_{p,q}(\dot{x^*_q} - \dot{x^*_p}) - I_{p,q}\big)^2, \tag{5}$$

where $\lambda \in (0.0, 1.0)$ is a control parameter, and $W_{p,q}$ is the *coupling strength*[1] between nodes p and q. When minimizing the first and second terms, the *intranode* and *internode* requirements are met maximally, respectively.

The dynamics and object function of the variable y_q are given as well as x_q:

$$\dot{y_q} = \sum_{p\in P_q} J_{p,q}, \tag{6}$$

$$H_J = \lambda \sum_{q\in Q} \Big(\dot{y^*_q} - g_q - \sum_{p\in P_q} J_{p,q}\Big)^2 + (1-\lambda) \sum_{(p,q)\in E} \big(W_{p,q}(\dot{y^*_q} - \dot{y^*_p}) - J_{p,q}\big)^2, \tag{7}$$

where $J_{p,q}$ is also a *current of resource*, and $g_q(t) \in \mathbb{R}$ is a variable to regulate the *growth* of the volume v_q, which will be explained later.

In this paper, we consider a four-node star network shown in Fig. 1C, where $Q = \{0, 1, 2, 3\}$, $E = \{(0, 1), (0, 2), (0, 3)\}$, $\lambda = 0.2$, and all coupling strengths are uniformly set as $W_{p,q} = 1$. Because the object functions H_I and H_J are quadratic, unique solutions for optimal currents $I_{p,q}$ and $J_{p,q}$ can be obtained analytically. Indeed, simultaneously solving equations $\frac{\partial H_I}{\partial I_{0,1}} = 0$, $\frac{\partial H_I}{\partial I_{0,2}} = 0$, and $\frac{\partial H_I}{\partial I_{0,3}} = 0$, we get the optimal currents $I_{0,1}$, $I_{0,2}$, and $I_{0,3}$ as follows:

$$\begin{aligned} I_{0,1/2/3} = \tfrac{1}{1+3\lambda}\Big(& W_{0,1/2/3}(\dot{x^*}_{1/2/3} - \dot{x^*_0}) \\ & -\lambda^2\big(-2\dot{x^*}_{1/2/3} + \dot{x^*}_{2/1/2} + \dot{x^*}_{3/3/1} - 2W_{0,1/2/3}(\dot{x^*}_{1/2/3} - \dot{x^*_0}) \\ & \quad - W_{0,2/1/2}(\dot{x^*}_{2/1/2} - \dot{x^*_0}) - W_{0,3/3/1}(\dot{x^*}_{3/3/1} - \dot{x^*_0})\big) \\ & +\lambda\big((1 + W_{0,1/2/3})(\dot{x^*}_{1/2/3} - \dot{x^*_0}) - W_{0,2/1/2}(\dot{x^*}_{2/1/2} - \dot{x^*_0}) \\ & \quad - W_{0,3/3/1}(\dot{x^*}_{3/3/1} - \dot{x^*_0})\big)\Big), \end{aligned} \tag{8}$$

where the subscript expression "1/2/3" indicates that three equations are collectively written. Similarly, we obtain the optimal currents $J_{0,1}$, $J_{0,2}$, and $J_{0,3}$:

$$\begin{aligned} J_{0,1/2/3} = \tfrac{1}{1+3\lambda}\Big(& W_{0,1/2/3}(\dot{y^*}_{1/2/3} - \dot{y^*_0}) \\ & -\lambda^2\big(-2g_{1/2/3} + g_{2/1/2} + g_{3/3/1} + 2\dot{y^*}_{1/2/3} - \dot{y^*}_{2/1/2} - \dot{y^*}_{3/3/1} \\ & \quad - 2W_{0,1/2/3}(\dot{y^*}_{1/2/3} - \dot{y^*_0}) + W_{0,2/1/2}(\dot{y^*}_{2/1/2} - \dot{y^*_0}) \\ & \quad + W_{0,3/3/1}(\dot{y^*}_{3/3/1} - \dot{y^*_0})\big) \\ & +\lambda\big(g_0 - g_{1/2/3} + (1 + W_{0,1/2/3})(\dot{y^*}_{1/2/3} - \dot{y^*_0}) \\ & \quad - W_{0,2/1/2}(\dot{y^*}_{2/1/2} - \dot{y^*_0}) - W_{0,3/3/1}(\dot{y^*}_{3/3/1} - \dot{y^*_0})\big)\Big). \end{aligned} \tag{9}$$

Substituting Eqs. (8), (9), (3), and (4) into Eqs. (2) and (6), the dynamics $\dot{x_q}$ and $\dot{y_q}$ are given as ordinary differential equations and can be solved numerically.

[1] It is possible to model the *asymmetry* in the influx and efflux of the *resource current* from node p to q. Indeed, replacing $W_{p,q}$ with a sigmoid function $(W_{p,q} - \epsilon) + \epsilon/(1 + Exp\{-\kappa(\dot{x^*_q} - \dot{x^*_p})\})$, the influx and efflux become uneven when $\epsilon > 0$ or $\epsilon < 0$.

2.2 Oscillation Modes

In this section, we fix all growth variables to be vanished as $g_q(t) = 0$ so that the amoeba's branch in each node never elongates nor withdraws (Fig. 1C). We introduce a parameter ρ to adjust the amplitude of the hub node 0 as $\sqrt{r_0} = 3\rho$, while that of the other terminal nodes are $\sqrt{r_1} = \sqrt{r_2} = \sqrt{r_3} = 3$. Depending on the hub's amplitude adjusted by ρ, the model produces different oscillation modes. In this study, we focus on six distinctive modes shown in Fig. 2, where for each mode we appropriately choose f to equalize the frequencies of all modes.

- **Mode 1: In-phase synchronization.** All terminal nodes 1, 2, and 3 synchronize in in-phase, but they synchronize with the hub node 0 in antiphase.
- **Mode 2: Partial in-phase synchronization A.** Two terminal nodes synchronize in in-phase, where the phases of these terminals are about 90° ahead of the other isolated terminal and are about 135° behind the hub. Because each of three terminals can be isolated, this mode gives three variations depending on initial states.
- **Mode 3: Partial in-phase synchronization B.** Two terminals perform in-phase synchronization, where the phases of these terminals are about 120° ahead of the other isolated terminal and are about 120° behind the hub. This mode also has three variations and is initial-state dependent.
- **Mode 4: Spontaneous mode switching.** The terminals spontaneously switch among three variations of the mode 3, as node 1, 3, and 2 are isolated cyclically in that order. Although each mode switches once every three periods, this behavior is not exactly periodic and produces a number of variations depending on initial states. The behavior is understood as complex quasi-periodic motion that appears to involve irregular fluctuations like *chaotic* behavior. We have also observed similar switching behavior in a model of a ring network of nonuniformly-coupled three oscillators and confirmed its mechanism to be the saddle node bifurcation. The *chaos-like* behavior was not strictly *chaos*, as the dynamics did not show the exponential divergence of neighboring points in the orbits. We will report these results elsewhere [15].
- **Mode 5: Long-term behavior.** Because the hub oscillates with the same amplitude as the terminals, the hub does not have enough capacity to absorb and emit the sum of resources flowing from the terminals within a single period. This leads the hub to oscillate 3/2 times as fast as the terminals and to have a large-scale trend varied in a long-term cycle, which requires 21 periods of oscillations. This mode also exhibits a number of variations.
- **Mode 6: Rotation.** Because the amplitude of the hub is much smaller than that of the terminals, the hub has only a small effect on resource traffic. The phase of each terminal differs equally about 120° from that of neighboring ones. That is, each terminal in turn transfers resources to its adjacent terminal in a manner similar to a unidirectional rotation movement. This mode has another variation to rotate in opposite direction.

The amoeba exhibited all these modes in experiments, but each mode continued for at most 10 periods and spontaneously switched to other modes, as reported in [7]. In this sense, the amoeba's behavior is best described by the mode 4.

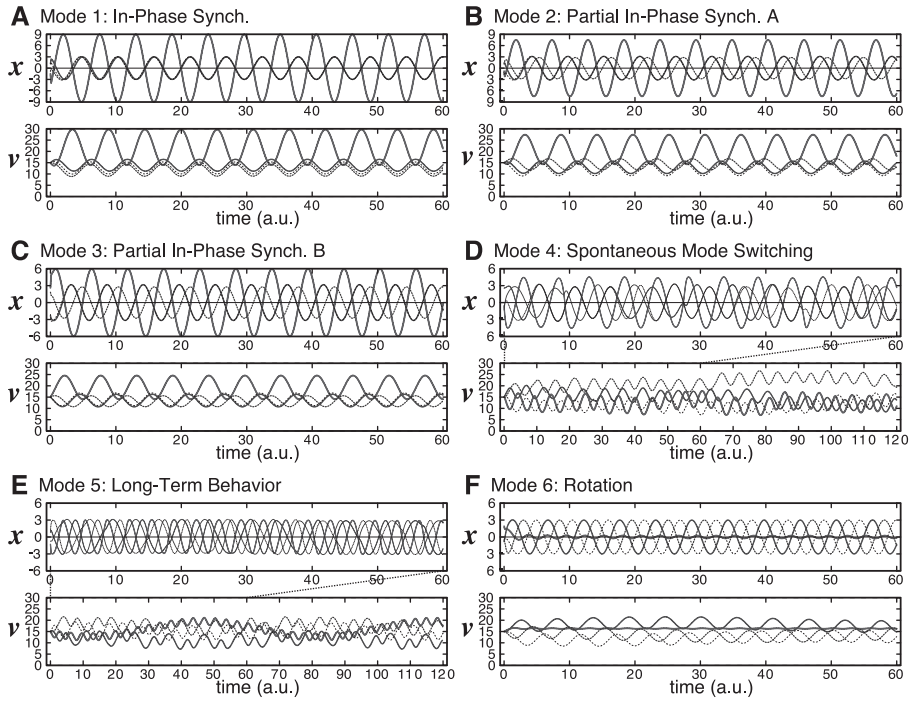

Fig. 2. Time series of six oscillation modes at $(\mu, \delta) = (0, 0)$ with initial states randomly chosen from $x_q \in [-3.0, 3.0]$ such that $\sum_{q \in Q} x_q = 0$, where $y_q = 0$ and $v_q = 15$. The thickest solid, second-thickest solid, dashed, and dotted lines correspond to the nodes 0, 1, 2, and 3, respectively. (A) In-phase synchronization at $(\rho, f) = (3, 0.456)$. (B) Partial in-phase synchronization A at $(\rho, f) = (2.5, 0.529)$. (C) Partial in-phase synchronization B at $(\rho, f) = (2, 0.628)$. (D) Spontaneous mode switching at $(\rho, f) = (1.5, 0.746)$. (E) Long-term behavior at $(\rho, f) = (1, 1)$. (F) Rotation at $(\rho, f) = (0.1, 1.139)$.

2.3 Growth and Degeneration of Branch

In our model depicted in Fig. 1D, the volume of each node v_q can be led to increase and decrease by setting the *growth variable* g_q to be positive and negative, respectively. Indeed, suppressing the increment of y_q by a positive g_q in Eq. (7), the increment of x_q is enhanced, and thus v_q grows. When x_q and y_q are considered to be the *activator* and *inhibitor* respectively, the effect of the positive g_q is taken as a process that the decrease of inhibitor yields the increase of activator.

The growth variable g_q gives the amoeba a force for pushing and pulling its branch, as it serves in a way comparable to the acceleration of the volume in Eq. (7). Assuming the sum of the amoeba's internally generated forces to be constant, we define g_q in a way similar to the Kirchhoff's laws Eqs. (2) and (6):

$$g_q = \sum_{p \in P_q} K_{p,q}, \tag{10}$$

where $K_{p,q}$ is called a *force transmission* from node p to q. As well as previously defined currents, *transmissions* $K_{p,q}$ are determined by minimizing the following object function H_K which balances intranode and internode requirements:

$$H_K = \sum_{q \in Q} \left(\mu \; s_q \; \hat{v}_q - \sum_{p \in P_q} K_{p,q}\right)^2 + \sum_{(p,q) \in E} \left(\delta \; W_{p,q}(\hat{v}_p - \hat{v}_q) - K_{p,q}\right)^2, \qquad (11)$$

where $\hat{v}_q = v_q/L$ is a *fraction of volume* divided by the *reference volume* $L = 40$. The first term of H_K models the effect of *intranode inhibitory stimulation* adjusted by $\mu \leq 0$ to reduce the volume when stimulated by light. In the next section, we will describe how to determine the *stimulation signal* s_q, which is a sort of on-off signal for indicating whether each node is illuminated ($s_q \simeq 1$) or not ($s_q \simeq 0$). The second term represents the effect of *internode diffusion* regulated by the parameter δ, which is a *diffusion coefficient* for tuning the reduction rate of the differences among the volumes of the nodes.

Solving $\frac{\partial H_K}{\partial K_{0,1}} = 0$, $\frac{\partial H_K}{\partial K_{0,2}} = 0$, and $\frac{\partial H_K}{\partial K_{0,3}} = 0$, the optimal transmissions $K_{p,q}$ can be obtained analytically as follows:

$$\begin{aligned} K_{0,1/2/3} = \tfrac{1}{10L}\Big(&-\mu\big(2s_0v_0 - 4s_{1/2/3}v_{1/2/3} + s_{2/1/2}v_{2/1/2} + s_{3/3/1}v_{3/3/1}\big) \\ &+ \delta\big(-4W_{0,1/2/3}(v_{1/2/3} - v_0) + W_{0,2/1/2}(v_{2/1/2} - v_0) \\ &+ W_{0,3/3/1}(v_{3/3/1} - v_0)\big)\Big). \end{aligned} \qquad (12)$$

There are dynamics $\dot{v_q}$, $\dot{x_q}$, and $\dot{y_q}$ given by Eqs. (1), (2), and (6), and we can rewrite these dynamics as ordinary differential equations by substituting analytic solutions of $I_{p,q}$, $J_{p,q}$, $K_{p,q}$ obtained as Eqs. (8), (9), and (12). Thus, numerical solutions for v_q, x_q, and y_q are obtained by routine procedures. This means that we can also calculate time series of $I_{p,q}$, $J_{p,q}$, $K_{p,q}$, and g_q.

Fig. 3 gives examples of the time series showing how the growth variable g_q works. In comparison with Fig. 3A showing a control condition $g_q(t) = 0$, it

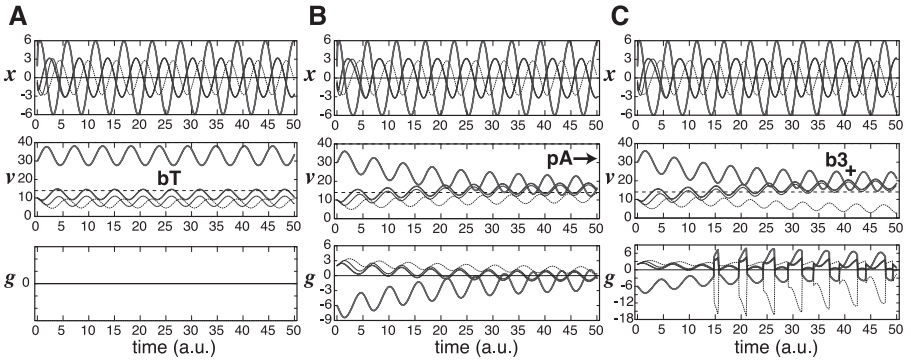

Fig. 3. Time series of the mode 3 at $(L, \theta) = (40, 0.35)$ with initial volumes $v_0 = 30$ and $v_1 = v_2 = v_3 = 10$. In v-panels, broken lines show the critical level $L\theta = 14$. (A) No growth at $(\mu, \delta) = (0, 0)$. (B) Volume diffusion at $(\mu, \delta) = (0, 20)$. (C) Problem-solving process at $(\mu, \delta) = (-200, 20)$. bT, pA, and $b3_+$ are explained in Fig. 4.

is confirmed in Fig. 3B that a large volume of the amoeba placed initially in the hub diffused into the terminal nodes as $g_0(t) < 0$, while the branches in the terminals grew as $g_1(t), g_2(t), g_3(t) > 0$. For all modes, the positive diffusion coefficient $\delta > 0$ brings about an effect to equalize the volumes of all nodes to oscillate around $\sum_{q\in Q} v_q(0)/M$ eventually.

2.4 Stress Minimization Problem in Volume Allocation

In previous works, the authors showed experimentally that the amoeba is useful for searching for solutions to the N-city TSP ($N = 4$ in [12,13]) in adopting the following discrete-time-state modified Hopfield-Tank model [16] to update s_q.

$$s_q(t + \Delta t) = 1 - Stp(\sum_{p\in Q} U_{p,q}\ sgm(\tilde{v}_p(t))), \tag{13}$$

where $s_q = 1$ if the light is on; otherwise 0, $\tilde{v}_q$ is an *area*[2] of the amoeba's branch in terminal node q, $sgm(\tilde{v}) = 1/(1 + Exp\{-b(\tilde{v} - \theta)\})$, and $Stp(V) = 0$ if $V < \Theta$; otherwise 1. Each terminal node $q \in Q$ is coupled with every node $(c, n) \in Q = \{c_1, c_2, \cdots, c_N\} \times \{1, 2, \cdots, N\}$ labeled with a *city name* c and its *visit order* n as

$$U_{(c,n),q} = \begin{cases} -\alpha & (\text{if } q = (c, n' \neq n) \text{ or } q = (c' \neq c, n)\ ), \\ -\beta\ dst(c, c') & (\text{if } q = (c' \neq c, n' \neq n) \text{ and } |n - n'| = 1\ ), \\ 0 & (\text{otherwise}), \end{cases} \tag{14}$$

where $dst(c, c')$ is a *distance* between c and c', and each *coupling weight* is *symmetric* ($U_{p,q} = U_{q,p}$). The optimal solution to the problem, the shortest travel to visit all cities, is expressed by the amoeba's stably relaxed shape that maximizes the body area while minimizing the risk of being stressed by light. The solution, therefore, would be the most comfortable condition for the amoeba and can be attained if the amoeba succeeds in elongating only the least-frequently stressed branches and withdrawing the other ones.

To determine which branches to grow, the amoeba needs to examine a lot of possible shapes (solutions) and to choose the minimally stressed one by comparing relative differences in the stressed frequencies of the candidates. It was observed that the amoeba examined a wide variety of shapes in a trial-and-error method by alternately expanding and shrinking its branches with its oscillatory behavior. That is, the oscillatory behavior was shown to be essential for the amoeba to attain the optimal solution because it enables the search of a broad solution space [12]. Although the amoeba exhibited various oscillation modes in the solution-searching processes, the dependence of the optimization performances on the oscillation modes remained unclear. In this paper, we use our model to compare the performances of the oscillation modes.

[2] In the experiments, the area $\tilde{v}_q$ was measured from a digital image taken at each interval $\Delta t = 6$ sec using a video camera. The *area* $\tilde{v}_q$ should be distinguished from the *volume* $\hat{v}_q$ considered in the model, because the sum of the latter is constant while that of the former is not.

We make minor revisions of the above scheme to be embedded in the continuous-time-state ordinary differential equations of our model as follows:

$$s_q = 1 - Sgm(\sum_{p \in P_q} U_{p,q}\ sgm(\hat{v}_p)), \tag{15}$$

where $Sgm(V) = 1/(1 + Exp\{-B(V - \Theta)\})$, $b = 35$, $\theta = 0.35$, $B = 1000$, and $\Theta = -0.5$. Additionally, we allow the weight matrix to be *asymmetric*:

$$\begin{pmatrix} U_{0,0}\ U_{0,1}\ U_{0,2}\ U_{0,3} \\ U_{1,0}\ U_{1,1}\ U_{1,2}\ U_{1,3} \\ U_{2,0}\ U_{2,1}\ U_{2,2}\ U_{2,3} \\ U_{3,0}\ U_{3,1}\ U_{3,2}\ U_{3,3} \end{pmatrix} = \begin{pmatrix} 0 & 0 & 0 & 0 \\ 0 & 0 & -0.3 & -0.3 \\ 0 & -0.4 & 0 & -0.3 \\ 0 & -0.2 & -0.3 & 0 \end{pmatrix}. \tag{16}$$

As we saw in Fig. 3B, in the absence of the feedback stimulation ($\mu = 0$), all terminal nodes grow beyond the critical level $L\theta$ to reach around $\sum_{q \in Q} v_q(0)/M$ due to the diffusion of the initial volume of the hub node. Namely, the hub volume is equally distributed to the terminals. On the other hand, when Eqs. (15) and (16) are substituted into Eq. (12) with $\mu < 0$, the feedback stimulation is implemented. As shown in Fig. 1D, a terminal node q is stimulated ($s_q \simeq 1$) if the other two terminals grow their volumes $v_{q'}$ and $v_{q''}$ to reach nearly the critical level $L\theta$. It is also confirmed in Fig. 3C that the feedback stimulation interferes the amoeba to elongate at most two branches while the other one is stressed by light .

As the growth of a branch brings to put certain levels of stresses on the other branches, the branches come into conflict over the allocation of the hub volume. We consider that this conflict presents a problem of finding an optimal way to allocate the hub volume to the terminals such that the total of stresses subjected to the amoeba can be minimized. We classify the *volume allocation patterns* by checking if each node is in sub-critical level ($v_q \leq L\theta$) or in super-critical level ($v_q > L\theta$). Accordingly, there are 16 patterns as shown in Fig. 4. We quantify the *stress level* as $\sum_{q \in Q} s_q \hat{v}_q$, because in the first term of Eq. (11) we assumed that each node is suppressed by a stress proportional to its volume when stimulated.

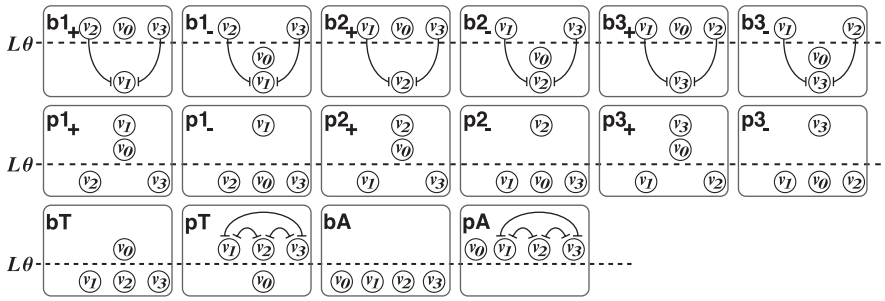

Fig. 4. Volume allocation patterns. Each circle over the critical level $L\theta$ (broken lines) represents $v_q > L\theta$, otherwise $v_q \leq L\theta$. Flat-headed arrows indicate inhibition by light.

3 Results

3.1 Diversities in Reachable Allocation Patterns

Typical examples of the problem-solving processes for all oscillation modes are shown in Fig. 5. For each mode, we carried out 100 trials of problem-solving processes started from the initial volumes $(v_0, v_1, v_2, v_3) = (45, 5, 5, 5)$ and random initial states $x_q \in [-3.0, 3.0]$ such that $\sum_{q \in Q} x_q = 0$, where $(\mu, \delta) = (-15, 10)$ and $(L, \theta) = (40, 0.35)$. For the pattern classification in each trial, we used time-averaged time series taken from $t = 1000$ to $t = 1500$. In almost all trials, the nodes finally reached a steady behavior that fell into one of the allocation patterns in Fig. 4, except for a few cases in the mode 4.

The histograms of the reached allocation patterns of all modes are shown in Fig. 6A. The modes 1, 2, 3, and 5 attained three patterns $b1_+, b2_+$, and $b3_+$, but their frequency distributions were different. The mode 6 did not reach any pattern other than pA in which all nodes are judged as slightly larger than the critical level after the time-averaging.

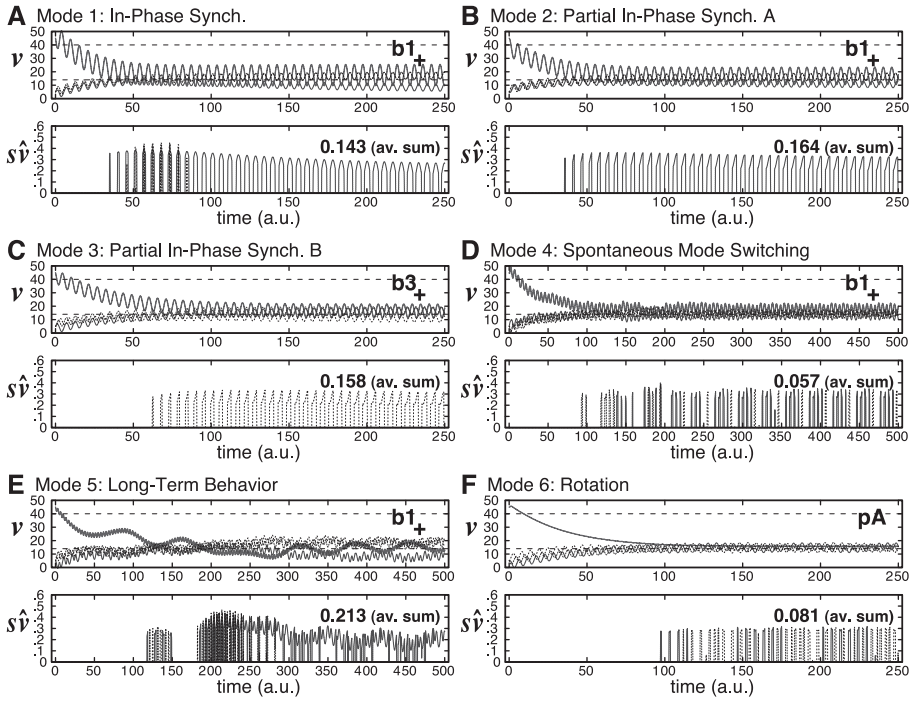

Fig. 5. Time series of problem-solving processes at $(\mu, \delta) = (-15, 10)$ and $(L, \theta) = (40, 0.35)$ with the initial volumes $(v_0, v_1, v_2, v_3) = (45, 5, 5, 5)$. In each v-panel, broken lines show the reference volume L and critical level $L\theta = 14$. In each $s\hat{v}$-panel, we showed the stress level $\sum_{q \in Q} s_q \hat{v}_q$ which was time-averaged after reaching a steady allocation pattern. For all modes, the parameters (ρ, f) were given as well as Fig.2.

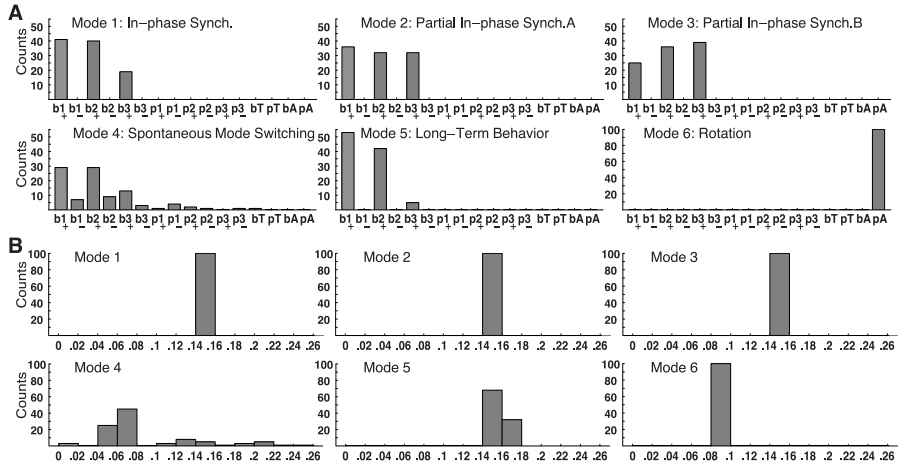

Fig. 6. Comparison of performances in diversity production (A) and stress minimization (B) among the oscillation modes. (A) Distributions of finally reached allocation patterns. (B) Distributions of time-averaged stress levels $\sum_{q\in Q} s_q \hat{v}_q$.

On the other hand, the mode 4, *spontaneous mode switching*, achieved 12 different patterns. Note that most of these patterns were not transient but were finally attained steady behavior. That is, the mode 4 is capable of not only searching for a large number of patterns but also maintaining each of these diverse patterns. Additionally, in a few cases, we observed *spontaneous transitions* among a number of patterns as shown in Fig. 7. This unstable transition behavior was likely to be a transient behavior before reaching a steady pattern.

3.2 Stress Minimization Capabilities

Fig. 6B shows the histograms of the *stress level* $\sum_{q\in Q} s_q \hat{v}_q$ achieved by all modes. For each mode, we analyzed the 100 trials of data used for Fig. 6A. The stress level shown here was time-averaged from $t = 1000$ to $t = 1500$, and it might be considered as a measure of discomfort felt by the amoeba resulting from conflicts among its branches. The stress levels of the modes 1, 2, 3, and 5 were relatively higher than that of the other modes. Namely, these modes maintained their allocation patterns in highly stressed ways. The mode 6 showed better performances in stress minimization, although it limits all nodes to have equally small volumes in the pattern pA.

The mode 4, *spontaneous mode switching*, produced the best stress minimization performances among all the modes. In most cases, the allocation patterns were maintained in less stressed ways compared with other modes. There existed a few stress-free cases in which no node was subjected to any stress while stably maintaining the pattern $p1_+$ or $p2_+$. On the other hand, there were some cases that were counted as highly stressed before reaching a steady pattern due to *spontaneous transition* among multiple patterns, as we saw in Fig. 7.

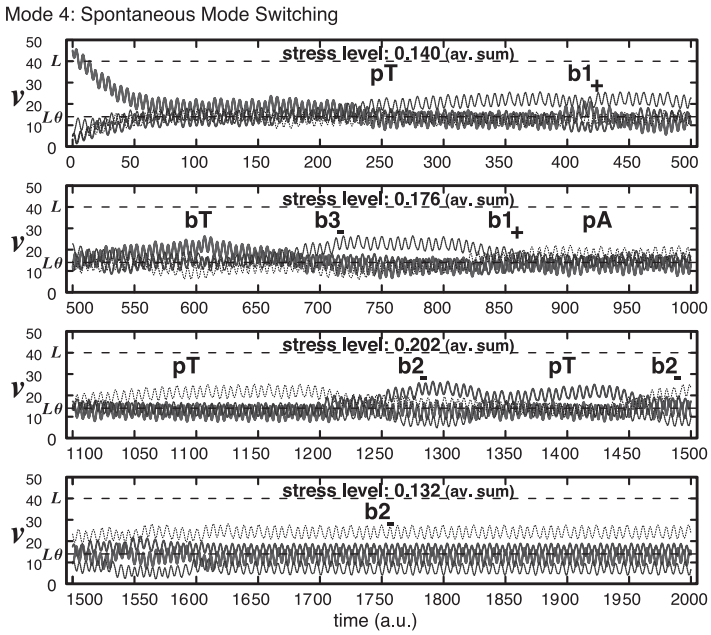

Fig. 7. An example of spontaneous transition among several volume allocation patterns produced by the mode 4. All parameters were set as well as Fig. 5.

4 Discussion and Conclusion

We presented a dynamical system model of the amoeba-based neurocomputer as a network of oscillators competing for limited resources. The model can be used for the solution search of various optimization problems of how to allocate limited resources to several nodes by minimizing the conflicts among the nodes. The resource allocation problem considered in this study is unique, because the problem should be solved under a looped constraint in which the system has to search for an optimal allocation pattern of a given resource (i.e., the amoeba's volume) by using the resource itself as the cost for the solution search (i.e., the growth movements of the amoeba's branches). Metaphorically speaking, the constraint is like a situation in which a consumer who tries to spend a certain amount of money usefully is requested to buy some products just to know their prices. That is, the history in information collecting process significantly influences the final decision on the solution. Therefore, it would be preferable that the time course of the process can be designed appropriately.

In order to cope with this unique problem, the model exploits the oscillatory behavior in the volumes of the nodes to perform deterministic trial and error for the solution search. The model produced a number of spatiotemporal oscillation modes, and these modes implemented different time courses of trial and error. We compared the performances of these modes in solving the problem. The

best performances were achieved by a complex mode in which the oscillators spontaneously switch among several modes.

The complex behavior reproduced well the amoeba's oscillatory behavior observed experimentally. Additionally, it resulted in spontaneous transition behavior among a number of solutions, which also looks similar to the amoeba's observed behavior in solving optimization problems [9,10,11,12,13]. In the experiments, after reaching a solution, the amoeba spontaneously destabilized the once-stabilized solution by elongating its branch under stressed condition and performed transition among multiple solutions. These similarities suggest that our model captures the essence of the amoeba's dynamics and will be a useful tool in exploring the origin and potential applications of the amoeba's computational capabilities.

Many natural, computing, economical, and social systems compete for limited resources and face problems similar to ours. In the absence of supervisor systems, these competitive systems need to discover optimal allocations in their own sophisticated trial-and-error methods. Our model is easily extended to model diverse competitive systems. Indeed, various dynamical systems can be coupled in the proposed form, and the object functions can be replaced freely by alternative ones as long as their optimal solutions can be obtained analytically. Thus, we expect that the framework of our model provides various insights for establishing efficient trial-and-error methods in a wide spectrum of competitive systems to solve the problems.

References

1. Nakagaki, T., Yamada, H., Toth, A.: Maze-Solving by an Amoeboid Organism. Nature 407, 470 (2000)
2. Tero, A., Kobayashi, R., Nakagaki, T.: Physarum solver: A biologically inspired method of road-network navigation. Physica A 363, 115–119 (2006)
3. Nakagaki, T., Iima, M., Ueda, T., Nishiura, Y., Saigusa, T., Tero, A., Kobayashi, R., Showalter, K.: Minimum-risk path finding by an adaptive amoebal network. Phys. Rev. Lett. 99, 068104 (2007)
4. Saigusa, T., Tero, A., Nakagaki, T., Kuramoto, Y.: Amoebae anticipate periodic events. Phys. Rev. Lett. 100, 018101 (2008)
5. Takamatsu, A., Fujii, T., Endo, I.: Time delay effect in a living coupled oscillator system with the plasmodium of Physarum polycephalum. Phys. Rev. Lett. 85, 2026–2029 (2000)
6. Takamatsu, A., Tanaka, R., Yamada, H., Nakagaki, T., Fujii, T., Endo, I.: Spatiotemporal symmetry in rings of coupled biological oscillators of Physarum plasmodial slime mold. Phys. Rev. Lett. 87, 078102 (2001)
7. Takamatsu, A.: Spontaneous switching among multiple spatio-temporal patterns in three-oscillator systems constructed with oscillatory cells of true slime mold. Physica D 223, 180–188 (2006)
8. Aono, M., Gunji, Y.-P.: Beyond input-output computings: Error-driven emergence with parallel non-distributed slime mold computer. BioSystems 71, 257–287 (2003)
9. Aono, M., Hara, M.: Amoeba-based Nonequilibrium Neurocomputer Utilizing Fluctuations and Instability. In: Aki, S.G., Calude, C.S., Dinneen, M.J., Rozenberg, G.,

Wareham, H.T. (eds.) UC 2007. LNCS, vol. 4618, pp. 41–54. Springer, Heidelberg (2007)
10. Aono, M., Hara, M., Aihara, K.: Amoeba-based Neurocomputing with Chaotic Dynamics. Commun. ACM 50(9), 69–72 (2007)
11. Aono, M., Hara, M.: Spontaneous deadlock breaking on amoeba-based neurocomputer. BioSystems 91, 83–93 (2008)
12. Aono, M., Hirata, Y., Hara, M., Aihara, K.: Amoeba-based chaotic neurocomputing: Combinatorial optimization by coupled biological oscillators. New Generation Computing 27, 129–157 (2009)
13. Aono, M., Hara, M., Aihara, K., Munakata, T.: Amoeba-based emergent computing: Combinatorial optimization and autonomous meta-problem solving. International Journal of Unconventional Computing (in press)
14. Kuznetsov, Y.A.: Elements of applied bifurcation theory. Springer, New York (2004)
15. Hirata, Y., Aono, M., Hara, M., Aihara, K.: Spontaneous mode switching in coupled oscillators competing for constant amounts of resources (submitted)
16. Hopfield, J.J., Tank, D.W.: Computing with Neural Circuits: A model. Science 233, 625–633 (1986)